



HAL
open science

Ferroelectric order versus metallicity in Sr $1-x$ Ca x TiO $3-\delta$ ($x = 0.009$)

Johannes Engelmayer, Xiao Lin, Fulya Koç, Christoph P Grams, Joachim Hemberger, Kamran Behnia, Thomas Lorenz

► To cite this version:

Johannes Engelmayer, Xiao Lin, Fulya Koç, Christoph P Grams, Joachim Hemberger, et al.. Ferroelectric order versus metallicity in Sr $1-x$ Ca x TiO $3-\delta$ ($x = 0.009$). *Physical Review B*, 2019, 10.1103/PhysRevB.100.195121 . hal-04036630

HAL Id: hal-04036630

<https://hal.science/hal-04036630>

Submitted on 19 Mar 2023

HAL is a multi-disciplinary open access archive for the deposit and dissemination of scientific research documents, whether they are published or not. The documents may come from teaching and research institutions in France or abroad, or from public or private research centers.

L'archive ouverte pluridisciplinaire **HAL**, est destinée au dépôt et à la diffusion de documents scientifiques de niveau recherche, publiés ou non, émanant des établissements d'enseignement et de recherche français ou étrangers, des laboratoires publics ou privés.

Ferroelectric order versus metallicity in $\text{Sr}_{1-x}\text{Ca}_x\text{TiO}_{3-\delta}$ ($x = 0.009$)

Johannes Engelmayr,¹ Xiao Lin,^{1,*} Fulya Koç,¹ Christoph P. Grams,¹

Joachim Hemberger,¹ Kamran Behnia,^{2,1} and Thomas Lorenz^{1,†}

¹*II. Physikalisches Institut, Universität zu Köln, Zùlpicher Str. 77, 50937 Köln, Germany*

²*Laboratoire de Physique et d'Étude des Matériaux (UMR 8213 CNRS-ESPCI),*

PSL Research University, 10 Rue Vauquelin, 75005 Paris, France

(Dated: July 24, 2019)

We report on a thermal-expansion study of the ferroelectric phase transition in insulating $\text{Sr}_{1-x}\text{Ca}_x\text{TiO}_3$ ($x = 0.009$) and its evolution upon increasing charge-carrier concentration up to $n \simeq 60 \times 10^{19} \text{ cm}^{-3}$. Although electric polarization is screened by mobile charge carriers, we find clear signatures of the ferroelectric phase transition in the thermal-expansion coefficient α of the weakly doped metallic samples. Upon increasing n , the transition temperature $T_C(n)$ and the magnitude of the anomalies in α rapidly decrease up to a threshold carrier density n^* above which broadened anomalies remain present. There is no indication for a sign change of α as is expected for a pressure-dependent quantum phase transition with n as the control parameter. Thus, the ferroelectriclike transition is either continuously fading away or it transforms to another low-temperature phase above n^* , but this change hardly affects the temperature-dependent $\alpha(T)$ data.

I. INTRODUCTION

Perovskite titanates ATiO_3 with divalent A -site ions contain tetravalent titanium with an empty $3d$ shell, such that these materials typically form band insulators. Some members of this $\text{A}^{2+}\text{Ti}^{4+}\text{O}_3$ family are ferroelectric such as BaTiO_3 , PbTiO_3 , CdTiO_3 ¹⁻⁴, whereas others like SrTiO_3 , CaTiO_3 , and EuTiO_3 show quantum paraelectric behavior⁵⁻¹¹, i.e., a ferroelectric long-range order is suppressed by quantum fluctuations. Although a ferroelectric transition is absent in both SrTiO_3 and CaTiO_3 ^{6,12}, mixing Sr and Ca on the A site ($\text{Sr}_{1-x}\text{Ca}_x\text{TiO}_3$) induces ferroelectricity already for tiny calcium substitutions $0.0018 \leq x < 0.02$ with increasing Curie temperature $T_C(x)$. For larger x , relaxor ferroelectric behavior is observed and finally the material becomes antiferroelectric above $x \simeq 0.12$ ¹³⁻¹⁷. The high-temperature structure of $\text{Sr}_{1-x}\text{Ca}_x\text{TiO}_3$ is cubic (space group $Pm\bar{3}m$, No. 221), but upon cooling it changes to the tetragonal, centrosymmetric space group $I4/mcm$ (No. 140) at an x -dependent transition temperature $T_s(x)$, which is significantly larger than the ferroelectric ordering temperature T_C . Because the finite polarization in the ferroelectric state requires the absence of an inversion center, the transition at T_C necessarily involves a further symmetry reduction. The crystal structure in the ferroelectric phase was found to belong to the orthorhombic point group $mm2$ ¹⁸⁻²⁰ and for $x = 0.02, 0.04$ the space group $Ic2m$ (No. 46) was specified by x-ray diffraction²¹.

Charge-carrier doping in pure SrTiO_3 by, e.g., a partial removal of oxygen or substitution of Sr (Ti) by La (Nb), induces metallic conductivity²²⁻²⁶ and, for certain carrier concentrations, even superconductivity^{27,28}. In systems with both, calcium substitution and electron doping ($\text{Sr}_{1-x}\text{Ca}_x\text{TiO}_{3-\delta}$), the T_C -related anomalies of the ferroelectric insulating parent compound persist within the metallic and superconducting phase^{29,30}.

Rischau *et al.* investigated the evolution of this ferroelectriclike transition with charge-carrier concentration n for $\text{Sr}_{1-x}\text{Ca}_x\text{TiO}_{3-\delta}$ with $x = 0.0022$ and $x = 0.009$ ³⁰. Based on minima in the resistivity data $\rho(T)$, a decreasing T_C upon increasing n was derived and a disappearance of the ferroelectriclike phase above a critical carrier density n_c that depends on the calcium content x . The mechanism behind this behavior remained unclear, but it was suggested that it could result from Friedel oscillations causing destructive interference of Ca-induced dipoles³⁰. In fact, such a mechanism was discussed theoretically already much earlier by Glinchuk *et al.*^{31,32}.

Rowley *et al.* discussed the appearance of ferroelectric order in insulating quantum paraelectrics in the context of quantum criticality³³ where for SrTiO_3 the quantum control parameter can be tuned either by stress³⁴, by chemical substitution like in $\text{Sr}_{1-x}\text{Ca}_x\text{TiO}_3$, or by oxygen-isotope exchange³⁵. In such a scenario, the charge-carrier concentration n represents an additional control parameter towards a metallic ground state. The presence of a quantum phase transition is intrinsically tied to a diverging Grüneisen parameter³⁶. For pressure-dependent quantum phase transitions, this holds for the Grüneisen ratio $\Gamma = \alpha/c_p$ with the thermal-expansion coefficient α and the specific heat c_p . In the vicinity of a quantum critical point Γ exhibits a sign change³⁷, which results from a sign change of α , because c_p is always positive³⁸. Experimentally, such sign changes of α are observed in diverse materials where the control parameter is either a magnetic field³⁹⁻⁴⁵, a chemical or hydrostatic pressure⁴⁶, or the charge-carrier concentration⁴⁷.

Here, we present a detailed study of the evolution of the ground state of $\text{Sr}_{1-x}\text{Ca}_x\text{TiO}_3$ with $x = 0.009$ as a function of the charge-carrier density n varying from the insulating parent compound to $n \simeq 6 \times 10^{20} \text{ cm}^{-3}$. Based on thermal-expansion measurements, we investigate the evolution of both the structural transition temperature T_s and the T_C -related transition as a function of carrier concentration n . With increasing n , T_s essen-

tially linearly decreases and the structural transition remains well defined over almost the entire doping range. In contrast, $T_C(n)$ and the corresponding anomalies in α rapidly decrease in the low- n range up to a threshold carrier concentration n^* , above which broadened anomalies remain present up to the highest n . There is no evidence for a sign change in α as a function of n . This either suggests the absence of a sharp quantum phase transition, because the ferroelectriclike transition in $\text{Sr}_{1-x}\text{Ca}_x\text{TiO}_3$ is continuously vanishing, e.g. by varying from long range to short range, or the symmetry of the low-temperature order changes at some critical charge-carrier content n^* without being directly reflected in the macroscopic uniaxial expansion $\alpha(T)$.

The discussion of our results is split into two parts. Section III A discusses the symmetry changes at the structural and the ferroelectric transition of the pristine insulating material in order to clarify how the macroscopic uniaxial expansion $\alpha(T)$ is related to a (partial) twinning occurring at both transitions, which sets the basis for the discussion of the evolution of both transitions as a function of the charge-carrier concentration in III B.

II. EXPERIMENTAL

A commercial $\text{Sr}_{1-x}\text{Ca}_x\text{TiO}_3$ single crystal with $x = 0.009$ was used for this study. The nominal Ca content was confirmed by secondary ion mass spectrometry (SIMS) as described in²⁹. The crystal was cut into cuboid pieces with all faces being cubic $\{100\}$ planes and dimensions optimized for Hall effect measurements (typically $0.5 \times 2.5 \times 5$ mm). In order to induce electron doping the samples were annealed under vacuum ($\lesssim 10^{-5}$ mbar) for 1 to 2 hours at temperatures between 700°C and 1000°C depending on the intended charge-carrier concentration. Resistivity and Hall effect measurements were carried out via a standard six-probe method using the commercial physical property measurement system (PPMS by QUANTUM DESIGN) and most of these data have been published in Ref.³⁰. On the same samples we studied the uniaxial thermal expansion by measuring the length change $\Delta L(T)$ using a home-built capacitance dilatometer. The samples were continuously heated from liquid-helium temperature to 180 K at a rate of about 0.1 K min^{-1} and the thermal-expansion coefficient $\alpha = (1/L_0)(\partial\Delta L/\partial T)$ was determined numerically. The heat-capacity measurement of pristine $\text{Sr}_{1-x}\text{Ca}_x\text{TiO}_3$ was performed using the microcalorimeter option of the PPMS.

III. RESULTS AND DISCUSSION

A. Pristine $\text{Sr}_{0.991}\text{Ca}_{0.009}\text{TiO}_3$

Figure 1 (a) shows the specific heat c_p/T of pristine $\text{Sr}_{0.991}\text{Ca}_{0.009}\text{TiO}_3$. The insets depict enlarged views of

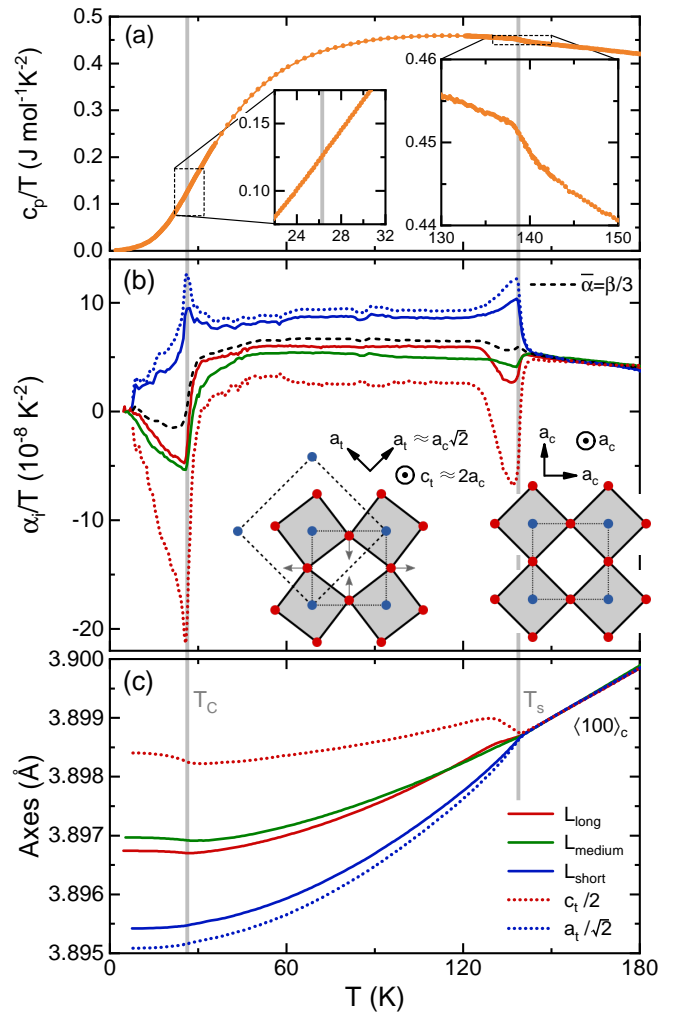


FIG. 1. (a) Specific heat c_p/T of pristine $\text{Sr}_{0.991}\text{Ca}_{0.009}\text{TiO}_3$. Insets show enlarged views around the structural and ferroelectric transition temperature T_S and T_C , respectively, both indicated by vertical lines. (b) Thermal-expansion coefficients α_i/T (thick lines) of pristine $\text{Sr}_{0.991}\text{Ca}_{0.009}\text{TiO}_3$ measured along the sample's dimensions L_i which are parallel to the cubic axes $\langle 100 \rangle$, together with the reconstructed α_i/T of the tetragonal axes $a_t/\sqrt{2}$ and $c_t/2$ (dotted lines) and average linear expansion $\bar{\alpha} = \beta/3$ (black dashed line). (c) Corresponding uniaxial length change $\Delta L_i/L_0$ adjusted to the cubic lattice parameter a_c measured at 150 K by x-ray diffraction⁴⁹. The sizes and orientations of the cubic and tetragonal unit cells of SrTiO_3 are sketched by the insets in (b) with blue (red) balls representing Ti (O) ions.

the temperature ranges around both the structural and ferroelectric transition temperature T_S and T_C , respectively, which were determined from thermal-expansion data [see Fig. 1 (b) and (c)]. In agreement with previous publications^{29,48} the structural transition at T_S is clearly visible by a small but distinct c_p anomaly, but no anomaly can be resolved in $c_p(T)$ around T_C .

Figure 1 (b) shows the thermal-expansion coefficients α_i/T of pristine $\text{Sr}_{0.991}\text{Ca}_{0.009}\text{TiO}_3$ measured along all

three of the cubic $\langle 100 \rangle$ directions (solid lines) that are parallel to the sample's dimensions L_i . Figure 1 (c) displays the corresponding uniaxial length changes $\Delta L_i/L_0$ adjusted to the cubic lattice parameter at 150 K⁴⁹. The α_i are identical at high temperatures and show pronounced anomalies around 139 K and 27 K. The upper temperature can be identified with the cubic-to-tetragonal transition temperature T_s . Pure SrTiO₃ becomes tetragonal around $T_s \simeq 105$ K⁵⁰⁻⁵³ and in Sr_{1-x}Ca_xTiO₃, T_s increases with increasing x ^{16,20,29,49,54}. The transition temperature $T_s \simeq 139$ K of our pristine sample with $x = 0.009$ is in agreement with findings in^{29,48,55}. The high-temperature cubic phase has the space group $Pm\bar{3}m$ (No. 221) while in the tetragonal phase it is $I4/mcm$ (140)⁵⁶. This transition is antiferrodistortive due to a tilting of the TiO₆ octahedra around the c axis⁵⁶⁻⁵⁸ corresponding to $(a^0a^0c^-)$ in the classification of Glazer^{59,60}, where a^0 denotes the absence of a tilting around the a axis and c^- represents an anti-phase tilting around the c axis. The inset in Fig. 1 (b) illustrates the octahedra tilt in a top view of the tetragonal ab plane. Titanium ions (blue) define the corners of the cubic unit cell (dotted square). At T_s , the oxygen ions (red) move as indicated by the arrows and consequently, the tetragonal unit cell (dashed square) is doubled in the ab plane and rotated by 45°. Due to the anti-phase tilting in c direction, the c axis is doubled as well. Thus, the cubic axes a_c and the tetragonal axes a_t, c_t are related by $a_t \approx \sqrt{2}a_c$ and $c_t \approx 2a_c$. It is evident, that the sample's dimensions L_i which are parallel to the cubic $\langle 100 \rangle$ directions, point along $\langle 110 \rangle$ with respect to the tetragonal axes a_t . The lower transition at 27 K signals the ferroelectric phase transition that was characterized by $P(E)$ hysteresis loops³⁰. While the structural transition at T_s is seen mainly in the sample's short direction L_{short} , the ferroelectric transition at T_C predominantly appears along the sample's medium and long direction L_{medium} and L_{long} , respectively.

Structural phase transitions generally involve transformation twinning^{61,62}. For a cubic-to-tetragonal transition one expects the emergence of three twin domains enabling different α_i to partially compensate each other. Therefore, a completely twinned sample should exhibit an isotropic uniaxial thermal expansion $\bar{\alpha}$, which is related to the volume expansion $\beta = 3\bar{\alpha}$. In general, $\beta = \sum_i \alpha_i$, where α_i denote the uniaxial expansion coefficients along a set of three pairwise orthogonal directions and for a tetragonal lattice, $\beta = 2\alpha_{a_t} + \alpha_{c_t}$ with the (usually anisotropic) main-axis expansion coefficients α_{a_t} and α_{c_t} along the tetragonal axes a_t and c_t , respectively. As shown by $\bar{\alpha} = \beta/3$ (black dashed line in Fig. 1 (b)), the transition at T_s is almost volume-conserving, i.e., the expansion in the long direction roughly compensates the contraction along the short and medium direction. A nearly volume-conserving transition is also reported for SrTiO₃ where the temperature-dependent lattice parameters around T_s were determined by high-resolution x-ray diffraction⁵². The anisotropic α_i and the nearly volume

conservation indicate highly unequal twinning fractions in our crystal. The usage of a capacitance dilatometer naturally requires the application of a certain uniaxial stress that can be sufficient to achieve a (partial) detwinning of the crystal^{63,64}. This is apparently not the case in our sample. Here, the presence of a dominating twin is not triggered by external conditions but rather predetermined by intrinsic crystal defects⁶⁵.

We can estimate the fraction of the tetragonal axes a_t and c_t along the sample's dimensions L_i by comparing the anomalies of the thermal-expansion coefficients of our measurements with the slope changes of the temperature-dependent lattice parameters around T_s from x-ray diffraction measurements. For this comparison, we use the high-resolution x-ray data of SrTiO₃⁵², which at T_s show an a_t -axis contraction that corresponds to a change $\Delta\alpha_a \simeq 8 \times 10^{-6} \text{ K}^{-1}$ and a c_t -axis expansion corresponding to $\Delta\alpha_c \simeq -16 \times 10^{-6} \text{ K}^{-1}$. By comparing these values to our thermal-expansion anomalies $\Delta\alpha_i$ at T_s we estimate that the sample's short axis L_{short} contains approximately $0.9a_t$ and $0.1c_t$, whereas the long axis contains $0.5a_t + 0.5c_t$, and the medium axis contains $0.6a_t + 0.4c_t$. From this estimate we reconstruct the tetragonal pure-axes compositions $a_t = 1.25L_{\text{short}} - 0.25L_{\text{long}}$ and $c_t = 2.25L_{\text{long}} - 1.25L_{\text{short}}$. Figures 1 (b) and (c) show the temperature-dependent behavior of the pure tetragonal axes $a_t/\sqrt{2}$ and $c_t/2$ as dotted lines. Of course, the derived anomalies $\Delta\alpha_a$ and $\Delta\alpha_c$ of Sr_{1-x}Ca_xTiO₃ at T_s are by construction identical to those observed by the temperature-dependent x-ray data of the SrTiO₃ lattice parameters⁵². The relation $\Delta\alpha_a \approx -\Delta\alpha_c/2$ is, however, independent from this reconstruction and directly follows from the (almost) absent anomaly in the volume expansion β and the tetragonal symmetry. In contrast to the transition at T_s , the ferroelectric transition at T_C is not volume conserving as is clearly demonstrated by the pronounced anomaly in the averaged uniaxial expansion $\bar{\alpha}$ (see black dashed line in Fig. 1 (b)). Furthermore, our reconstructed pure-axis data suggest that the volume-expansion anomaly essentially arises from a c -axis expansion upon cooling below T_C , while the transition is roughly area-conserving with respect to the ab plane. The latter is naturally expected for a tetragonal-to-orthorhombic transition with opposite expansion anomalies of similar magnitudes along the orthorhombic a and b axes. Note that the ferroelectric polarization is expected to be aligned along one of these orthorhombic axes, as it has been discussed in^{13,21,66}. In this context, it is also worth to mention that a tetragonal-to-orthorhombic transition increases the number of possible twin domains by a factor of two. However, the uniaxial length change measured along the tetragonal $[110]$ direction cannot distinguish between multi-domain and single-domain orthorhombic samples, because $\alpha_{[110]} = (\alpha_a + \alpha_b)/2$ in both cases.

B. Electron-doped samples $\text{Sr}_{0.991}\text{Ca}_{0.009}\text{TiO}_{3-\delta}$

Figure 2 shows the thermal-expansion coefficients α/T versus T of $\text{Sr}_{0.991}\text{Ca}_{0.009}\text{TiO}_{3-\delta}$ with different charge-carrier concentrations up to $n \leq 57.9 \times 10^{19} \text{ cm}^{-3}$ together with α/T of the pristine sample already shown in Fig. 1. For clarity, the curves are shifted by $7.5 \times 10^{-8} \text{ K}^{-2}$ with respect to each other. On each sample, we measured α_i along L_{long} . Since all samples were obtained by parallel cuts from the original single crystal it appears plausible that the distribution of twin domains does not vary too much over the individual samples. This assumption is essentially confirmed by the fact that all samples, apart from the one with highest n , show clear anomalies of the same sign and similar shape signaling the structural phase transition at T_s . With increasing n the transition temperature linearly decreases from $T_s \simeq 139 \text{ K}$ in pristine $\text{Sr}_{0.991}\text{Ca}_{0.009}\text{TiO}_3$ to $\simeq 116 \text{ K}$ for $n = 22.6 \times 10^{19} \text{ cm}^{-3}$ [see Fig. 3 (b)]. A linear decreasing $T_s(n)$ is known from reduced $\text{SrTiO}_{3-\delta}$ ^{67–69} and a decreased T_s was also seen in reduced $\text{EuTiO}_{3-\delta}$ ¹¹, suggesting that this is a generic trend in these almost cubic perovskite titanates⁷⁰. An extrapolation of the linear $T_s(n)$ dependence to the highest doping $n = 57.9 \times 10^{19} \text{ cm}^{-3}$ matches the kink at 80 K in the α/T curve of the corresponding sample. This suggests that the structural transition remains present in the entire series of $\text{Sr}_{0.991}\text{Ca}_{0.009}\text{TiO}_{3-\delta}$ samples, but the highest-doped sample apparently has an essentially homogeneous distribution of twin domains and, consequently, the averaged uniaxial expansion $\bar{\alpha}$ hardly shows any anomaly at this volume-conserving transition as discussed above.

The transition at T_C is clearly identifiable for the lower-doped samples (left panel of Fig. 2) and shifts from $T_C \simeq 27 \text{ K}$ for pristine $\text{Sr}_{0.991}\text{Ca}_{0.009}\text{TiO}_3$ down to 18 K for $n = 1.3 \times 10^{19} \text{ cm}^{-3}$. For the higher-doped samples (right panel of Fig. 2) the α/T anomalies become much less pronounced and rather broad; except for the sample with $n = 12.4 \times 10^{19} \text{ cm}^{-3}$. Despite this broadening a signature of the transition remains present in α/T of all doped samples. For example, in the more homogeneously twinned sample with $n = 57.9 \times 10^{19} \text{ cm}^{-3}$ the clear minimum of $\bar{\alpha}/T$ around 17 K signals the spontaneous volume expansion resulting from the low-temperature transition, whereas $\bar{\alpha}/T$ only shows a kink at T_s of the high-temperature structural transition, which is volume conserving.

Figure 3 compares the evolution of both transition temperatures T_s and T_C as a function of charge-carrier density n . The linear shift of T_s and the weak broadening of the structural transition with increasing n indicate that both the distribution of oxygen vacancies and the resulting charge-carrier density are rather homogeneous in the studied samples. Nevertheless, the low-temperature transition shows a complex behavior. The ferroelectric transition of the insulating pristine sample causes a very sharp α/T anomaly, which remains sharp

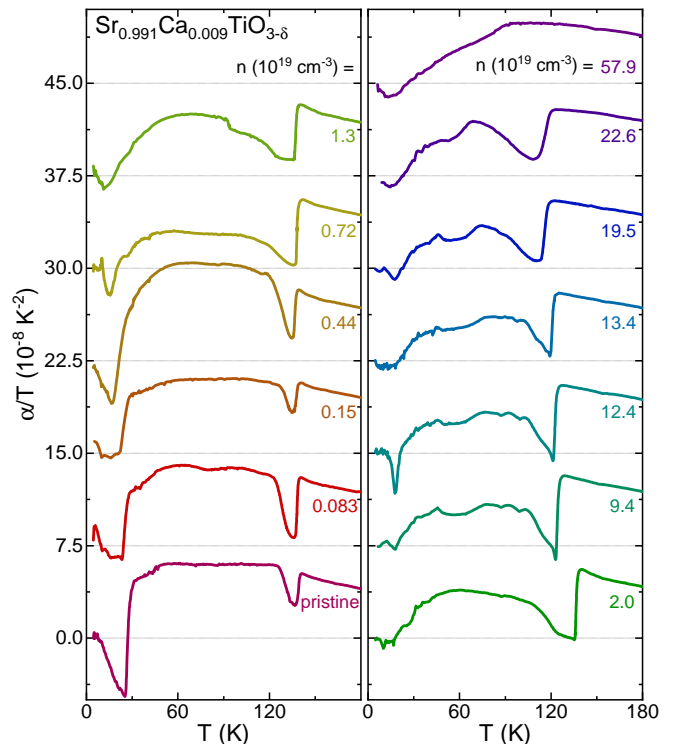


FIG. 2. Thermal-expansion coefficient α/T versus T of $\text{Sr}_{0.991}\text{Ca}_{0.009}\text{TiO}_{3-\delta}$ with different carrier densities n . Curves are shifted with respect to each other.

for the low-doped metallic samples but broadens above $n = 1.3 \times 10^{19} \text{ cm}^{-3}$. As a criterion to define T_C , we take the maximum slope of α/T and use the temperature difference to the minimum of α/T as a measure of the transition width, which is shown as error bars in Fig. 3 (a,b). The corresponding $T_C(n)$ curve is concave for $n \leq 1.3 \times 10^{19} \text{ cm}^{-3}$, as indicated by the dotted line in Fig. 3 (a) and essentially saturates for larger n . As a further measure of this transition, we use a smooth background α_{bg} and calculate $\varepsilon = \int (\alpha - \alpha_{\text{bg}}) dT$, which yields the spontaneous elongation resulting from the low-temperature transition. For $\alpha_{\text{bg}}(T)$ we measured the thermal expansion α_{STO} on a single crystal of SrTiO_3 ⁷¹, which remains in the tetragonal phase and scaled this $\alpha_{\text{STO}}(T)$ curve such that it matches $\alpha(T \approx 25 \text{ K})$ of the respective $\text{Sr}_{0.991}\text{Ca}_{0.009}\text{TiO}_{3-\delta}$ sample. This is shown for 2 exemplary charge-carrier contents in Fig. 3 (e,f) and the resulting $\varepsilon(T)$ are displayed in Fig. 3 (g) with every second measurement skipped for clarity. The evolution of $\varepsilon(T = 4.2 \text{ K}, n)$ as a function n is summarized in Fig. 3 (c,d); the corresponding error bars express the sensitivity of $\varepsilon(T = 4.2 \text{ K}, n)$ on variations of the individual scaling factors used for α_{STO} . We see that $\varepsilon(T = 4.2 \text{ K}, n)$ rapidly decreases at $n \leq 1.3 \times 10^{19} \text{ cm}^{-3}$ and then levels off at a value of about 15% of the spontaneous elongation measured in the ferroelectric phase of pristine $\text{Sr}_{0.991}\text{Ca}_{0.009}\text{TiO}_3$. This behavior is qualitatively similar to that of $T_C(n)$, which saturates, however,

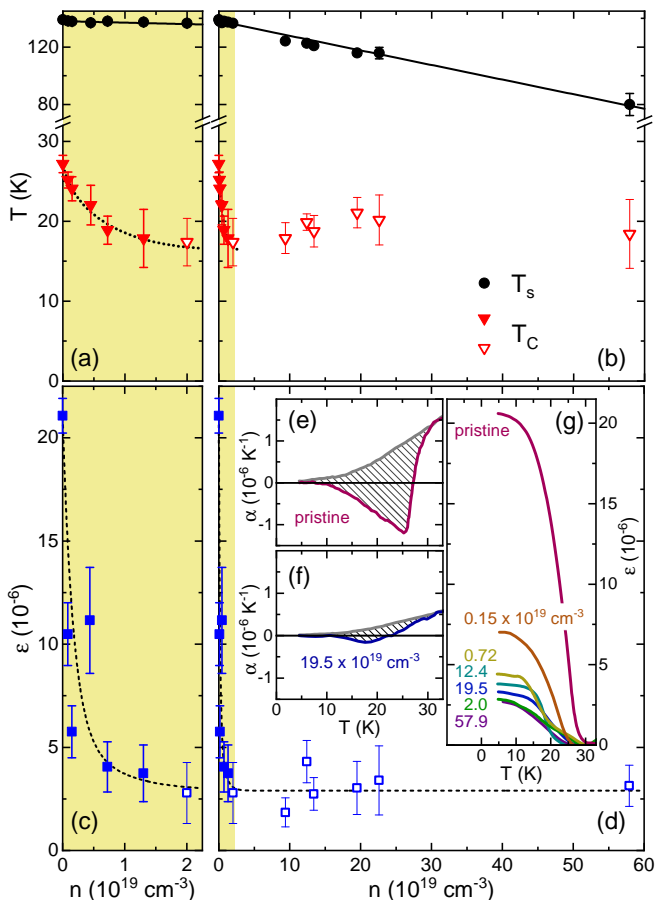


FIG. 3. Phase diagram of $\text{Sr}_{0.991}\text{Ca}_{0.009}\text{TiO}_{3-\delta}$. Open symbols refer to weak anomalies. (a) Detail view of the low- n regime with guide to the eye for $T_C(n)$ (dotted curve). (b) Complete range of n with linear fit of $T_s(n)$ (black solid line). Note the scale breaks in panels (a) and (b). (c, d) Spontaneous strain ϵ as a function of n . (e, f) We used $\alpha(T)$ of pure SrTiO_3 as background (gray curves) and integrated the difference to $\alpha(T)$ of the respective $\text{Sr}_{0.991}\text{Ca}_{0.009}\text{TiO}_{3-\delta}$ sample, exemplary shown for $n = 0$ (e) and $n = 19.5 \times 10^{19} \text{ cm}^{-3}$ (f). (g) Temperature dependence of ϵ of selected samples.

at a comparatively larger value of about 60% of T_C of the insulating pristine material.

These are the main findings of the present study, which extends our previous work suggesting the existence of a ferroelectric quantum phase transition inside the superconducting dome of $\text{Sr}_{1-x}\text{Ca}_x\text{TiO}_{3-\delta}$ ³⁰. As already discussed there, a true ferroelectric order cannot exist in metals, because the mobile electrons screen any static electric polarization. However, characteristic features of the ferroelectric order in $\text{Sr}_{1-x}\text{Ca}_x\text{TiO}_3$ are still observed upon weak charge-carrier doping suggesting a ferroelectriclike transition that vanishes via a quantum phase transition as indicated by minima in the resistivity data $\rho(T, n)$ ³⁰. The aim of the present study was to further clarify this issue via thermal-expansion measurements, which are a sensitive thermodynamic probe to detect and characterize pressure-dependent quantum

phase transitions^{36,37,39–47}. The existence of a well-defined ferroelectriclike transition in the metallic samples is clearly confirmed by the pronounced α/T anomalies (see Fig. 2) up to at least $n = 0.72 \times 10^{19} \text{ cm}^{-3}$, i.e., the transition remains present in metallic samples which finally become superconducting at lower temperature³⁰. On further increasing n , however, the α/T anomalies do not vanish and, in particular, our data do not give any indication for a sign change of the α/T anomalies as a function of n . Thus, the general behavior of α and the corresponding Grüneisen ratio $\Gamma = \alpha/c_p$ is different from other materials showing quantum phase transitions as a function of magnetic field, pressure, or n as external control parameter^{39–47}. On the one hand, this could mean the absence of a quantum phase transition, if the ferroelectriclike order changes just continuously disappears towards larger n . On the other hand, however, it is also clear from Figs. 2 and 3 that the shape and width of the α/T anomalies strongly change around $n = 1.3 \times 10^{19} \text{ cm}^{-3}$. This could mean that the symmetry change of the structural transition is different above and below a critical doping n^* in the range of $1.3 \times 10^{19} \text{ cm}^{-3}$. A similar situation is, in fact, observed in the undoped $\text{Sr}_{1-x}\text{Ca}_x\text{TiO}_3$ where, as a function of x , the symmetry of the low-temperature ordered phase changes from polar ferroelectric (space group $Ic2m$; No. 46) via relaxor ferroelectric to antiferroelectric with inversion symmetry ($Pbcm$, No. 57) above $x \simeq 0.12$ ^{13–17}. Such a microscopic change is not necessarily reflected in the thermal-expansion coefficient. In the simplest case, this could be an experimental problem, because a more or less vertical phase boundary in an n - T phase diagram is difficult to measure as a function of T . More generally, anomalies in the uniaxial expansion α require a finite dependence of the respective transition temperature on uniaxial stress along this direction⁷². In this context, it is also important that the polarization of $\text{Sr}_{1-x}\text{Ca}_x\text{TiO}_3$ is in the orthorhombic ab plane^{13,21,66}, such that a change of the in-plane symmetry will have minor influence on the observed α/T anomaly, because it arises from a spontaneous elongation of the c -axis component in our partially twinned crystals, as discussed above in the context of Fig. 1. Thus, detailed structural analysis of the low-temperature phases for different charge-carrier concentrations would be necessary to resolve this puzzle.

IV. SUMMARY

In conclusion, we present a detailed thermal-expansion study on $\text{Sr}_{1-x}\text{Ca}_x\text{TiO}_{3-\delta}$ ($x = 0.009$) with charge-carrier density tuned from the pristine, insulating parent compound to $n \simeq 60 \times 10^{19} \text{ cm}^{-3}$. Both the cubic-to-tetragonal transition T_s and the ferroelectric transition T_C display pronounced anomalies in the thermal-expansion coefficient $\alpha(T)$ of the pristine crystal. As a function of charge-carrier density n , T_s decreases linearly from 139 K to 80 K and the related anomalies in α/T

remain distinct and of similar magnitude across almost the entire doping range. Despite the presence of mobile charge carriers, the T_C -related anomaly survives for $n > 0$. However, T_C decreases rapidly upon increasing n and the associated anomalies in α/T become very broad above $n \simeq 1.3 \times 10^{19} \text{ cm}^{-3}$. Whether the evolution of T_C across this carrier concentration is continuous or passes a phase transition at a critical n^* is not directly seen in $\alpha(T)$ but needs to be clarified by a structure analysis.

ACKNOWLEDGMENTS

We acknowledge support by the DFG (German Research Foundation) via project number 277146847 - CRC 1238 (Subprojects A02, B01 and B02). This work is part of a DFG-ANR project funded by Agence Nationale de la Recherche (ANR-18-CE92-0020-01) and by the DFG through projects LO 818/6-1 and HE 3219/6-1. X. L. acknowledges support by the Alexander von Humboldt Foundation and Zhejiang Provincial Natural Science Foundation of China under Grant No. LQ19A040005.

-
- * Present address: School of Science, Westlake University, 18 Shilongshan Road, 310024, Hangzhou, China
 † tl@ph2.uni-koeln.de
- ¹ A. von Hippel, Ferroelectricity, Domain Structure, and Phase Transitions of Barium Titanate, *Rev. Mod. Phys.* **22**, 221 (1950).
 - ² V. G. Bhide, K. G. Deshmukh, and M. S. Hegde, Ferroelectric properties of PbTiO_3 , *Physica* **28**, 871 (1962).
 - ³ P.-H. Sun, T. Nakamura, Y. J. Shan, Y. Inaguma, and M. Itoh, The study on the dielectric property and structure of perovskite titanate CdTiO_3 , *Ferroelectrics* **217**, 137 (1998).
 - ⁴ B. J. Kennedy, Q. Zhou, and M. Avdeev, The ferroelectric phase of CdTiO_3 : A powder neutron diffraction study, *J. Solid State Chem.* **184**, 2987 (2011).
 - ⁵ T. Nakamura, P.-H. Sun, Y. J. Shan, Y. Inaguma, M. Itoh, I.-S. Kim, J.-H. Sohn, M. Ikeda, T. Kitamura, and H. Konagaya, On the perovskite-related materials of high dielectric permittivity with small temperature dependence and low dielectric loss, *Ferroelectrics* **196**, 205 (1997).
 - ⁶ I.-S. Kim, M. Itoh, and T. Nakamura, Electrical conductivity and metal-nonmetal transition in the perovskite-related layered system $\text{Ca}_{n+1}\text{Ti}_n\text{O}_{3n+1-\delta}$ ($n = 2, 3, \infty$), *J. Solid State Chem.* **101**, 77 (1992).
 - ⁷ V. V. Lemanov, A. V. Sotnikov, E. P. Smirnova, M. Weihnacht, and R. Kunze, Perovskite CaTiO_3 as an incipient ferroelectric, *Solid State Commun.* **110**, 611 (1999).
 - ⁸ K. A. Müller and H. Burkard, SrTiO_3 : An intrinsic quantum paraelectric below 4 K, *Phys. Rev. B* **19**, 3593 (1979).
 - ⁹ T. Katsufuji and H. Takagi, Coupling between magnetism and dielectric properties in quantum paraelectric EuTiO_3 , *Phys. Rev. B* **64**, 054415 (2001).
 - ¹⁰ S. Kamba, D. Nuzhnyy, P. Vaněk, M. Savinov, K. Knížek, Z. Shen, E. Šantavá, K. Maca, M. Sadowski, and J. Petzelt, Magnetodielectric effect and optic soft mode behaviour in quantum paraelectric EuTiO_3 ceramics, *Europhys. Lett.* **80**, 27002 (2007).
 - ¹¹ J. Engelmayer, X. Lin, C. P. Grams, R. German, T. Fröhlich, J. Hemberger, K. Behnia, and T. Lorenz, Charge transport in oxygen-deficient EuTiO_3 : The emerging picture of dilute metallicity in quantum-paraelectric perovskite oxides, *Phys. Rev. Materials* **3**, 051401(R) (2019).
 - ¹² J. K. Hulm, The Dielectric Properties of some Alkaline Earth Titanates at Low Temperatures, *Proc. Phys. Soc. London, Sect. A* **63**, 1184 (1950).
 - ¹³ J. G. Bednorz and K. A. Müller, $\text{Sr}_{1-x}\text{Ca}_x\text{TiO}_3$: An XY Quantum Ferroelectric with Transition to Randomness, *Phys. Rev. Lett.* **52**, 2289 (1984).
 - ¹⁴ R. Ranjan, D. Pandey, and N. P. Lalla, Novel Features of $\text{Sr}_{1-x}\text{Ca}_x\text{TiO}_3$ Phase Diagram: Evidence for Competing Antiferroelectric and Ferroelectric Interactions, *Phys. Rev. Lett.* **84**, 3726 (2000).
 - ¹⁵ R. Ranjan and D. Pandey, Antiferroelectric phase transition in $(\text{Sr}_{1-x}\text{Ca}_x)\text{TiO}_3$ ($0.12 < x \leq 0.40$): I. Dielectric studies, *J. Phys.: Condens. Matter* **13**, 4239 (2001).
 - ¹⁶ R. Ranjan and D. Pandey, Antiferroelectric phase transition in $(\text{Sr}_{1-x}\text{Ca}_x)\text{TiO}_3$: II. X-ray diffraction studies, *J. Phys.: Condens. Matter* **13**, 4251 (2001).
 - ¹⁷ S. K. Mishra, R. Ranjan, D. Pandey, and B. J. Kennedy, Powder neutron diffraction study of the antiferroelectric phase transition in $\text{Sr}_{0.75}\text{Ca}_{0.25}\text{TiO}_3$, *J. Appl. Phys.* **91**, 4447 (2002).
 - ¹⁸ U. Bianchi, W. Kleemann, and J. G. Bednorz, Raman scattering of ferroelectric $\text{Sr}_{1-x}\text{Ca}_x\text{TiO}_3$, $x = 0.007$, *J. Phys.: Condens. Matter* **6**, 1229 (1994).
 - ¹⁹ W. Kleemann, A. Albertini, M. Kuss, and R. Lindner, Optical detection of symmetry breaking on a nanoscale in $\text{SrTiO}_3\text{:Ca}$, *Ferroelectrics* **203**, 57 (1997).
 - ²⁰ M. A. Carpenter, C. J. Howard, K. S. Knight, and Z. Zhang, Structural relationships and a phase diagram for $(\text{Ca,Sr})\text{TiO}_3$ perovskites, *J. Phys.: Condens. Matter* **18**, 10725 (2006).
 - ²¹ S. K. Mishra and D. Pandey, Low temperature x-ray diffraction study of the phase transitions in $\text{Sr}_{1-x}\text{Ca}_x\text{TiO}_3$ ($x = 0.02, 0.04$): Evidence for ferrielectric ordering, *Appl. Phys. Lett.* **95**, 232910 (2009).
 - ²² H. P. R. Frederikse, W. R. Thurber, and W. R. Hosler, Electronic Transport in Strontium Titanate, *Phys. Rev.* **134**, A442 (1964).
 - ²³ O. N. Tufte and P. W. Chapman, Electron Mobility in Semiconducting Strontium Titanate, *Phys. Rev.* **155**, 796 (1967).
 - ²⁴ H. P. R. Frederikse and W. R. Hosler, Hall mobility in SrTiO_3 , *Phys. Rev.* **161**, 822 (1967).
 - ²⁵ C. Lee, J. Destry, and J. L. Brebner, Optical absorption and transport in semiconducting SrTiO_3 , *Phys. Rev. B* **11**, 2299 (1975).
 - ²⁶ A. Spinelli, M. A. Torija, C. Liu, C. Jan, and C. Leighton, Electronic transport in doped SrTiO_3 : Conduction mechanisms and potential applications, *Phys. Rev. B* **81**, 155110 (2010).

- ²⁷ J. F. Schooley, W. R. Hosler, and M. L. Cohen, Superconductivity in semiconducting SrTiO₃, *Phys. Rev. Lett.* **12**, 474 (1964).
- ²⁸ X. Lin, G. Bridoux, A. Gourgout, G. Seyfarth, S. Krämer, M. Nardone, B. Fauqué, and K. Behnia, Critical doping for the onset of a two-band superconducting ground state in SrTiO_{3- δ} , *Phys. Rev. Lett.* **112**, 207002 (2014).
- ²⁹ B. S. de Lima, M. S. da Luz, F. S. Oliveira, L. M. S. Alves, C. A. M. dos Santos, F. Jomard, Y. Sidis, P. Bourges, S. Harms, C. P. Grams, J. Hemberger, X. Lin, B. Fauqué, and K. Behnia, Interplay between antiferrodistortive, ferroelectric, and superconducting instabilities in Sr_{1-x}Ca_xTiO_{3- δ} , *Phys. Rev. B* **91**, 045108 (2015).
- ³⁰ C. W. Rischau, X. Lin, C. P. Grams, D. Finck, S. Harms, J. Engelmayer, T. Lorenz, Y. Gallais, B. Fauqué, J. Hemberger, and K. Behnia, A ferroelectric quantum phase transition inside the superconducting dome of Sr_{1-x}Ca_xTiO_{3- δ} , *Nat. Phys.* **13**, 643 (2017).
- ³¹ M. D. Glinchuk and I. V. Kondakova, Ruderman-Kittel-like interaction of electric dipoles in systems with carriers, *phys. stat. sol. (b)* **174**, 193 (1992).
- ³² M. D. Glinchuk, I. V. Kondakova, and R. O. Kuzian, The possibility of Kondo-like effect in systems with non-tunneling off-center ions, *Ferroelectrics* **153**, 97 (1994).
- ³³ S. E. Rowley, L. J. Spalek, R. P. Smith, M. P. M. Dean, M. Itoh, J. F. Scott, G. G. Lonzarich, and S. S. Saxena, Ferroelectric quantum criticality, *Nat. Phys.* **10**, 367 (2014).
- ³⁴ H. Uwe and T. Sakudo, Stress-induced ferroelectricity and soft phonon modes in SrTiO₃, *Phys. Rev. B* **13**, 271 (1976).
- ³⁵ M. Itoh, R. Wang, Y. Inaguma, T. Yamaguchi, Y.-J. Shan, and T. Nakamura, Ferroelectricity Induced by Oxygen Isotope Exchange in Strontium Titanate Perovskite, *Phys. Rev. Lett.* **82**, 3540 (1999).
- ³⁶ L. Zhu, M. Garst, A. Rosch, and Q. Si, Universally Diverging Grüneisen Parameter and the Magnetocaloric Effect Close to Quantum Critical Points, *Phys. Rev. Lett.* **91**, 066404 (2003).
- ³⁷ M. Garst and A. Rosch, Sign change of the Grüneisen parameter and magnetocaloric effect near quantum critical points, *Phys. Rev. B* **72**, 205129 (2005).
- ³⁸ The divergence and sign change of α/c_p require a finite pressure dependence of the underlying quantum phase transition, which, for example, may result from a pressure-dependent quantum critical magnetic field.
- ³⁹ R. Küchler, N. Oeschler, P. Gegenwart, T. Cichorek, K. Neumaier, O. Tegus, C. Geibel, J. A. Mydosh, F. Steglich, L. Zhu, and Q. Si, Divergence of the Grüneisen Ratio at Quantum Critical Points in Heavy Fermion Metals, *Phys. Rev. Lett.* **91**, 066405 (2003).
- ⁴⁰ P. Gegenwart, F. Weickert, M. Garst, R. S. Perry, and Y. Maeno, Metamagnetic Quantum Criticality in Sr₃Ru₂O₇ Studied by Thermal Expansion, *Phys. Rev. Lett.* **96**, 136402 (2006).
- ⁴¹ J. Baier, P. Steffens, O. Schumann, M. Kriener, S. Stark, H. Hartmann, O. Friedt, A. Revcolevschi, P. G. Radaelli, S. Nakatsuji, Y. Maeno, J. A. Mydosh, T. Lorenz, and M. Braden, Magnetoelastic Coupling Across the Metamagnetic Transition in Ca_{2-x}Sr_xRuO₄ (0.2 \leq x \leq 0.5), *J. Low Temp. Phys.* **147**, 405 (2007).
- ⁴² T. Lorenz, S. Stark, O. Heyer, N. Hollmann, A. Vasiliev, A. Oosawa, and H. Tanaka, Thermodynamics of the coupled spin-dimer system TlCuCl₃ close to a quantum phase transition, *J. Magn. Magn. Mater.* **316**, 291 (2007).
- ⁴³ T. Lorenz, O. Heyer, M. Garst, F. Anfuso, A. Rosch, C. Rüegg, and K. Krämer, Diverging Thermal Expansion of the Spin-Ladder System (C₅H₁₂N)₂CuBr₄, *Phys. Rev. Lett.* **100**, 067208 (2008).
- ⁴⁴ O. Breunig, M. Garst, E. Sela, B. Buldmann, P. Becker, L. Bohatý, R. Müller, and T. Lorenz, Spin- $\frac{1}{2}$ XXZ Chain System Cs₂CoCl₄ in a Transverse Magnetic Field, *Phys. Rev. Lett.* **111**, 187202 (2013).
- ⁴⁵ O. Breunig, M. Garst, A. Klümper, J. Rohrkamp, M. M. Turnbull, and T. Lorenz, Quantum criticality in the spin-1/2 Heisenberg chain system copper pyrazine dinitrate, *Sci. Adv.* **3**, eaa03773 (2017).
- ⁴⁶ K. Grube, L. Pintschovius, F. Weber, J.-P. Castellan, S. Zaum, S. Kuntz, P. Schweiss, O. Stockert, S. Bachus, Y. Shimura, V. Fritsch, and H. v. Löhneysen, Magnetic and Structural Quantum Phase Transitions in CeCu_{6-x}Au_x are Independent, *Phys. Rev. Lett.* **121**, 087203 (2018).
- ⁴⁷ C. Meingast, F. Hardy, R. Heid, P. Adelman, A. Böhmer, P. Burger, D. Ernst, R. Fromknecht, P. Schweiss, and T. Wolf, Thermal Expansion and Grüneisen Parameters of Ba(Fe_{1-x}Co_x)₂As₂: A Thermodynamic Quest for Quantum Criticality, *Phys. Rev. Lett.* **108**, 177004 (2012).
- ⁴⁸ E. McCalla, J. Walter, and C. Leighton, A Unified View of the Substitution-Dependent Antiferrodistortive Phase Transition in SrTiO₃, *Chem. Mater.* **28**, 7973 (2016).
- ⁴⁹ S. K. Mishra, R. Ranjan, D. Pandey, P. Ranson, R. Ouilon, J.-P. Pinan-Lucarre, and P. Pruzan, A combined X-ray diffraction and Raman scattering study of the phase transitions in Sr_{1-x}Ca_xTiO₃ (x = 0.04, 0.06, and 0.12), *J. Solid State Chem.* **178**, 2846 (2005).
- ⁵⁰ L. Rimai and G. A. deMars, Electron Paramagnetic Resonance of Trivalent Gadolinium Ions in Strontium and Barium Titanates, *Phys. Rev.* **127**, 702 (1962).
- ⁵¹ F. W. Lytle, X-Ray Diffractometry of Low-Temperature Phase Transformations in Strontium Titanate, *J. Appl. Phys.* **35**, 2212 (1964).
- ⁵² N. Ohama, H. Sakashita, and A. Okazaki, The temperature dependence of the lattice constant of SrTiO₃ around the 105 K transition, *Phase Transit.* **4**, 81 (1984).
- ⁵³ M. Sato, Y. Soejima, N. Ohama, A. Okazaki, H. J. Scheel, and K. A. Müller, The lattice constant vs. temperature relation around the 105 K transition of a flux-grown SrTiO₃ crystal, *Phase Transit.* **5**, 207 (1985).
- ⁵⁴ T. Mitsui and W. B. Westphal, Dielectric and X-Ray Studies of Ca_xBa_{1-x}TiO₃ and Ca_xSr_{1-x}TiO₃, *Phys. Rev.* **124**, 1354 (1961).
- ⁵⁵ V. V. Lemanov, Phase transitions in SrTiO₃-based solid solutions, *Phys. Solid State* **39**, 1468 (1997).
- ⁵⁶ H. Unoki and T. Sakudo, Electron Spin Resonance of Fe³⁺ in SrTiO₃ with Special Reference to the 110°K Phase Transition, *J. Phys. Soc. Jpn.* **23**, 546 (1967).
- ⁵⁷ P. A. Fleury, J. F. Scott, and J. M. Worlock, Soft Phonon Modes and the 110°K Phase Transition in SrTiO₃, *Phys. Rev. Lett.* **21**, 16 (1968).
- ⁵⁸ G. Shirane and Y. Yamada, Lattice-Dynamical Study of the 110°K Phase Transition in SrTiO₃, *Phys. Rev.* **177**, 858 (1969).
- ⁵⁹ A. M. Glazer, The classification of tilted octahedra in perovskites, *Acta Crystallogr. Sect. B* **28**, 3384 (1972).
- ⁶⁰ A. M. Glazer, Simple ways of determining perovskite structures, *Acta Crystallogr. Sect. A* **31**, 756 (1975).
- ⁶¹ R. W. Cahn, Twinned crystals, *Adv. Phys.* **3**, 363 (1954).
- ⁶² A. Authier, ed., *International Tables for Crystallography, Volume D*, 1st ed. (International Union of Crystallography,

- 2003).
- ⁶³ S. K. Niesen, G. Kolland, M. Seher, O. Breunig, M. Vallador, M. Braden, B. Grenier, and T. Lorenz, Magnetic phase diagrams, domain switching, and quantum phase transition of the quasi-one-dimensional Ising-like antiferromagnet $\text{BaCo}_2\text{V}_2\text{O}_8$, *Phys. Rev. B* **87**, 224413 (2013).
- ⁶⁴ S. Kunkemöller, D. Brünig, A. Stunault, A. A. Nugroho, T. Lorenz, and M. Braden, Magnetic shape-memory effect in SrRuO_3 , *Phys. Rev. B* **96**, 220406(R) (2017).
- ⁶⁵ When measuring along L_{long} , the force applied via the dilatometer acts on the smallest cross-sectional area of our sample and consequently produces the largest pressure, whereas along L_{short} the force acts on the largest cross section producing the smallest pressure. Nevertheless, we observe an expansion along L_{long} and a compression along L_{short} when cooling across T_s , which indicates the absence of stress-induced detwinning.
- ⁶⁶ W. Kleemann, F. J. Schäfer, K. A. Müller, and J. G. Bednorz, Domain state properties of the random-field xy-model system $\text{Sr}_{1-x}\text{Ca}_x\text{TiO}_3$, *Ferroelectrics* **80**, 297 (1988).
- ⁶⁷ D. Bäuerle and W. Rehwald, Structural phase transitions in semiconducting SrTiO_3 , *Solid State Commun.* **27**, 1343 (1978).
- ⁶⁸ D. Wagner, D. Bäuerle, F. Schwabl, B. Dorner, and H. Kraxenberger, Soft modes in semiconducting SrTiO_3 – I. The Zone Boundary Mode, *Z. Phys. B* **37**, 317 (1980).
- ⁶⁹ Q. Tao, B. Loret, B. Xu, X. Yang, C. W. Rischau, X. Lin, B. Fauqué, M. J. Verstraete, and K. Behnia, Nonmonotonic anisotropy in charge conduction induced by antiferrodistortive transition in metallic SrTiO_3 , *Phys. Rev. B* **94**, 035111 (2016).
- ⁷⁰ The decrease of T_s is, however, not a direct consequence of the charge-carrier doping, because n -type doping by chemical substitution like in $\text{SrTi}_{1-x}\text{Nb}_x\text{O}_3$ increases T_s ^{48,69}.
- ⁷¹ On our twinned SrTiO_3 crystal we find a smooth $\alpha(T)$ low-temperature behavior. In contrast, thermal-expansion data on SrTiO_3 measured under strong uniaxial compressive stress result in single-domain tetragonal samples with very different expansion⁷³. The corresponding $\alpha(T)$ curves show a minimum between 20 K and 30 K, which resembles the data of our Ca-doped samples. Because SrTiO_3 is known to develop a stress-induced ferroelectric order³⁴, the anomalous $\alpha(T)$ curves observed in⁷³ probably arise from ferroelectric order that is induced in those SrTiO_3 crystals by the application of the uniaxial compressive stress.
- ⁷² This follows from general thermodynamics via Clausius-Clapeyron (Ehrenfest) relations for first- (second-)order phase transitions.
- ⁷³ S. Tsunekawa, H. F. J. Watanabe, and H. Takei, Linear thermal expansion of SrTiO_3 , *phys. stat. sol. (a)* **83**, 467 (1984).